Numerical Simulation Analysis of Seismic Performance of Adjustable High-Strength Tie Rods

Miaofa Xu [1], Zhanzhong Yin [1,2], Yongsheng Mao [3,*], Youtao Zhu [1]

[1] School of Civil Engineering, Lanzhou University of Science and Technology, Lanzhou, China

[2] Ministry of Education Engineering Research Center for Civil Engineering Disaster Prevention and Mitigation, Lanzhou University of Science and Technology, Lanzhou, China

[3] Gansu Institute of Architectural Design and Research Co., ·Ltd

* Corresponding Author Email: 1348810467@qq.com

Abstract. To address the buckling susceptibility and inadequate energy dissipation capacity of conventional braces, this study proposes a novel Buckling-Restrained Brace (BRB) integrated with movable high-strength tie rods. Eight finite element models were developed using ABAQUS to systematically investigate the effects of core tube slenderness ratio, tie rod configuration, and core tube-to-tie rod area ratio on the mechanical performance, including load-bearing capacity and energy dissipation characteristics. The results demonstrate that under low-cycle reversed loading, the proposed brace exhibits stable and well-developed hysteresis loops, smooth skeleton curves, and superior ductility with significant plastic deformation capacity. Notably, the brace displays significantly enhanced stiffness and strength in tension compared to compression. This tension-compression asymmetry provides theoretical foundations for optimizing innovative composite bracing systems.

Keywords: High-strength tie rods, Numerical simulation, Buckling-Restrained Brace, Hysteretic behavior.

1. Introduction

Pure steel frame structures are prone to structural instability under horizontal loads due to insufficient lateral stiffness. To address this deficiency, structural systems such as steel plate shear walls and composite bracing systems have emerged in recent years. While steel plate shear walls overcome the limited ductility of concrete shear walls and exhibit inherent robustness, they remain susceptible to out-of-plane instability during loading. To mitigate these issues, traditional steel braces and shear plates have been integrated into steel frames to form composite bracing systems [1]. Although these systems enhance lateral stiffness, their stability under moderate-to-severe earthquakes remains inadequate, often leading to global instability or local buckling, which significantly compromises structural ductility and energy dissipation capacity. To prevent such buckling failures, researchers have proposed various improvements to optimize the mechanical performance of steel braces [2-4]. Studies have demonstrated that while these enhanced braces exhibit mechanical properties similar to conventional ones, their cumulative plastic deformation and energy dissipation capabilities are markedly superior.

Buckling-restrained braces (BRBs) [5-9], as energy-dissipating components, enable the core member to yield in both tension and compression without buckling. A typical BRB consists of an axial force-resisting core and an external restraining assembly that suppresses core buckling under compression by providing lateral constraint [10-12]. In response to the global instability issues of traditional steel braces, researchers worldwide have extensively investigated BRBs. Guo Yanlin et al. [13] elaborated on the composition, working principles, analytical methods, and global applications of BRBs, establishing a theoretical foundation for their development. However, BRBs are primarily employed in composite bracing systems alongside other energy-dissipating elements. Gu Luzhong et al. [14] implemented BRBs in concrete frames and conducted quasi-static tests, revealing excellent collaborative performance, stable hysteresis loops, and enhanced structural damping for energy dissipation. Wu Hui et al. [15] applied BRBs to multi-story structures, with seismic tests confirming

improved seismic performance, as BRBs absorbed the majority of earthquake energy. Nevertheless, excessive out-of-plane instability may still occur under horizontal loading. Building upon the dual-tube restrained buckling brace [16], this study introduces two movable high-strength tie rods to develop a novel constrained buckling brace with adjustable tie rods. When integrated into frame structures, this brace forms an innovative composite bracing system. Under horizontal loading, the core tube and tie rods along the tension diagonal jointly participate in energy dissipation, while the tie rods remain inactive in compression, effectively mitigating out-of-plane instability. Internal Construction Diagram of the Brace shown in Figure 1.

Using the ABAQUS nonlinear finite element platform, a systematic numerical study was conducted on eight BRB models with varying design parameters. This investigation focused on the influence of core tube slenderness ratio, high-strength tie rod configuration, and core tube-to-tie rod cross-sectional area ratio on ultimate bearing capacity, hysteretic energy dissipation, and failure modes. Results demonstrate that the proposed brace exhibits stable bilinear hysteretic behavior under cyclic loading, with the synergistic interaction of high-strength tie rods effectively suppressing local buckling. These findings provide theoretical and parametric foundations for the seismic-resilient design of high-performance composite bracing systems.

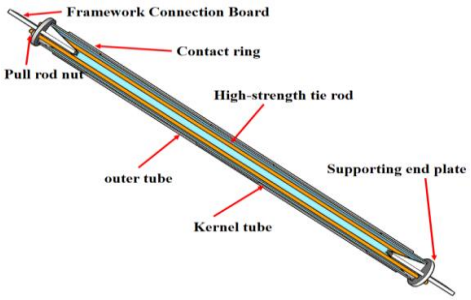

Figure 1. Internal construction of the brace

2. Finite Element Modeling

2.1. Model Development

Numerical simulations were performed using ABAQUS finite element software. All components were modeled with 8-node linear brick elements (C3D8R). The cross-sectional dimensions of the core tube, contact ring, and outer restraining tube were Φ60×3.5 mm, Φ68×4.0 mm, and Φ76×4.0 mm, respectively. Q235B steel was adopted for all components except the high-strength tie rods (Q355/Q460/Q620 steel). Detailed geometric parameters of the models are listed in Table 1.

Table 1. Geometric parameters of analytical models

Model	Core tube length (m)	Outer tube length (m)	Tie rod diameter (mm)	Steel grade
BRB-1	1.2	1.1	10	Q355
BRB-2	2.4	2.1	10	Q355
BRB-3	2.4	2.1	10	Q355
BRB-4	2.4	2.1	12	Q460
BRB-5	2.4	2.1	14	Q620
BRB-6	2.0	1.9	10	Q355
BRB-7	2.0	1.9	-	-
BRB-8	2.4	2.1	-	-

2.2. Material Constitutive Model and Initial Imperfection Modeling

The material constitutive model defined the steel properties with an elastic modulus E=200GPa (2.0×10^5 MPa), Poisson's ratioν=0.3, and additional mechanical parameters (yield strength, ultimate strength, and elongation at fracture Ω) as detailed in Table 2. The von Mises yield criterion was

adopted to describe elastoplastic behavior, with an idealized elastoplastic constitutive model simulating post-yield mechanical response. While this simplification effectively characterizes structural plastic development, abrupt stiffness transitions may introduce numerical convergence challenges. To account for geometric imperfections in actual components, the equivalent geometric imperfection method was applied by imposing an initial lateral displacement perturbation of L/1000 (L: member length) at the mid-span, simulating the coupled effects of residual stresses and initial curvature.

Table 2. Material properties

Material	ε_y(MPa)	ε_u	σ_y(MPa)	σ_u	E(GPa)	Ω/%
Q235B	271	0	522	0.20	200	25

2.3. Contact Definitions and Loading Protocol

Contact interactions were defined with tangential behavior governed by the Coulomb friction model and normal behavior using the hard contact formulation. To address geometric nonlinearity-induced overclosure issues under large deformations, the augmented Lagrange algorithm with automatic overclosure adjustment was implemented. Boundary conditions included: Fixed end: Fully constrained (ENCASTRE: Ux=Uy=Uz=0), Loading end: Constrained out-of-plane displacement (Uz=0) while releasing rotational degrees of freedom about the Ux-axis. Kinematic coupling constraints were applied to link the degrees of freedom (Ux, Uy, ROTz) of end-plate nodes to a reference point (RP-1), establishing a quasi-rigid loading boundary (Figure 2). Following Chinese civil engineering testing specifications [17], a displacement-controlled protocol with incrementally increasing amplitudes was adopted, where tensile and compressive phases corresponded to positive and negative displacement amplitudes, respectively (Figure 3). Geometric nonlinearity (NLGEOM) was activated in the numerical model to ensure convergence during large deformation analysis.

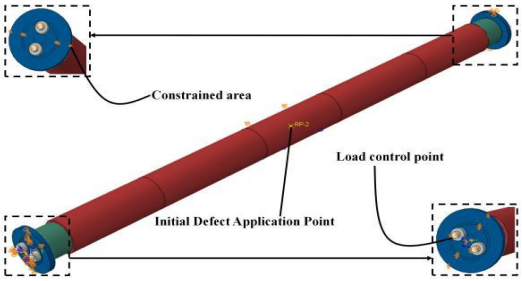

Figure 2. Boundary conditions

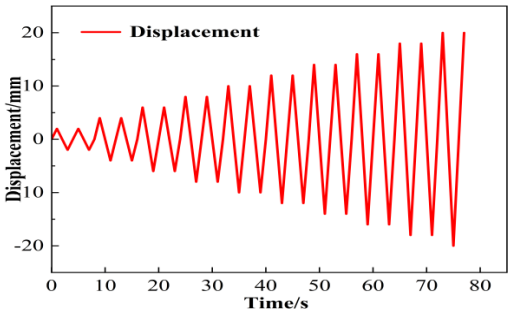

Figure 3. Loading protocol

3. Finite Element Results and Analysis

3.1. Characteristics of Hysteretic Behavior

Figure 4 illustrates the hysteretic curves of the specimens under cyclic loading. For models BRB-7 and BRB-8 without tie rods (Figure 4c), symmetric hysteresis loops are observed. As the

displacement amplitude increases, the hysteresis loops gradually expand. However, in later loading stages, the compressive hysteresis loops exhibit inward pinching due to necking of the core tube.In contrast, the specimens with tie rods (Figures 4a and 4b) demonstrate peak-enhanced tensile hysteresis loops, where the tensile peak load significantly exceeds the compressive peak load. This behavior results from the combined action of the core tube and high-strength tie rods under tension, while the tie rods remain inactive during compression.

Key observations from Figure 4c indicate that the inclusion of tie rods increases the hysteresis loop area, thereby enhancing the plastic deformation capacity and energy dissipation performance of the brace. The peak-enhancement in tensile hysteresis loops is attributed to the substantial improvement in strength and stiffness when both the core tube and tie rods resist tensile forces. Meanwhile, the compressive hysteresis loops remain relatively stable due to stress redistribution, which delays necking development.Analysis of Figure 4a reveals that increasing the slenderness ratio of the core tube initially enlarges the hysteresis loop area. However, further increases in slenderness ratio lead to a reduction in loop area and promote inward pinching under compression. This occurs because while greater core tube length enhances axial deformation capacity, excessive slenderness ratios induce higher-order buckling modes, causing local instability and impairing both axial deformation and energy dissipation. Therefore, controlling the slenderness ratio is essential for optimal energy dissipation performance.As shown in Figure 4b, the compressive hysteresis loops remain consistent, while the tensile hysteresis loop area increases slightly with decreasing core tube-to-tie rod area ratio. However, the overall variation is limited, indicating that the area ratio primarily influences tensile performance through stiffness redistribution, with minimal impact on compressive behavior.

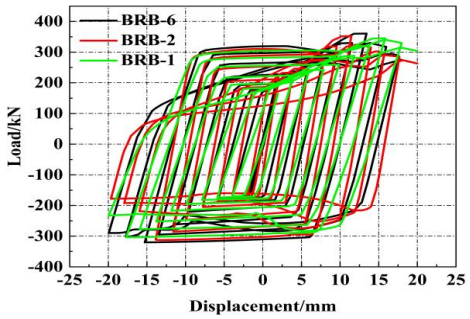

(a) Core Member Slenderness Ratio

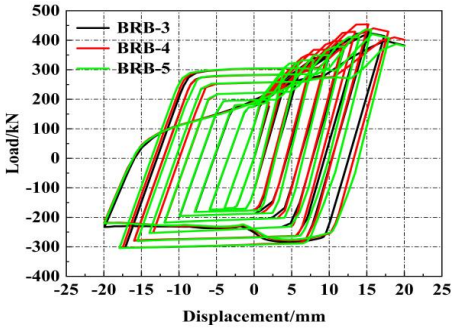

(b) Area ratio of the core tube to the tie rod

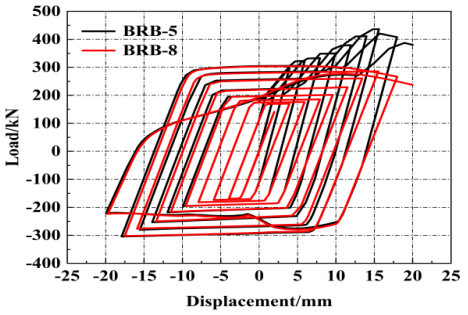

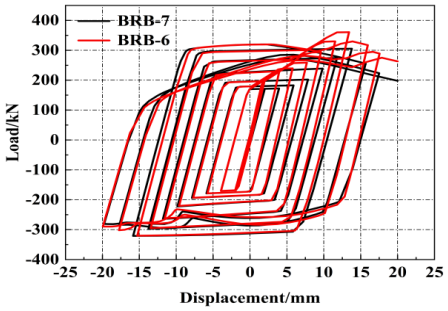

(c) Presence of tie rods

Figure 4. Hysteresis curves of the specimens

3.2. Energy Dissipation Capacity Evaluation

The energy dissipation capacity of the structural members can be quantified by the enclosed area of the hysteresis loops (as shown in Figure 5), represented by the energy dissipation coefficient E. The calculation formula for the energy dissipation coefficient [18] is as follows:

$$E = \frac{S_{ABC+CDA}}{S_{ODG+OBH}}$$

Where $S_{ABC+CDA}$ is the area enclosed by the hysteresis loop, Δ_{ODG} and Δ_{OBH} is the $S_{ODG+OBH}$ of the areas.

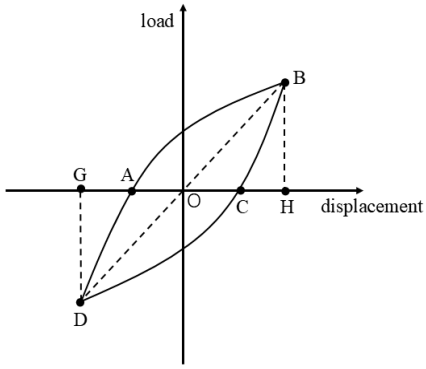

Figure 5. Calculation method of energy dissipation coefficient

In accordance with the Specification for Seismic Testing of Buildings [19], this study adopts the equivalent energy dissipation coefficient E as the key indicator for evaluating the seismic performance of structural members. Analysis of the energy dissipation coefficient curves (Figure 6) reveals that all restrained buckling brace specimens equipped with movable tie rods satisfy the requirement of E≥2.0 at loading termination, achieving the "excellent" energy dissipation grade specified by the code.

As shown in Figure 6a, the energy dissipation coefficient increases with growing displacement amplitudes. During later loading stages, the coefficient stabilizes before ultimately decreasing due to local buckling of the core tube. Moderate increases in slenderness ratio can enhance energy dissipation capacity by improving member ductility. However, excessive slenderness ratios may trigger premature buckling, primarily because the increased slenderness ratio lengthens the tie rods, thereby affecting the overall stiffness and strength characteristics that govern energy dissipation performance.Figure 6b demonstrates the influence of core tube-to-tie rod area ratio on energy dissipation capacity. The consistent development trend of energy dissipation coefficients indicates that the area ratio has limited impact on energy dissipation performance. However, during later loading stages, core tube necking reduces load-bearing capacity and consequently energy dissipation, with the area ratio's influence becoming more pronounced during this necking phase.Figure 6c illustrates the effect of tie rod installation on energy dissipation performance. While the tie rod configuration significantly improves structural strength and stiffness, it also moderately restricts full development of plastic deformation as displacement amplitudes increase, compared to specimens without tie rods.

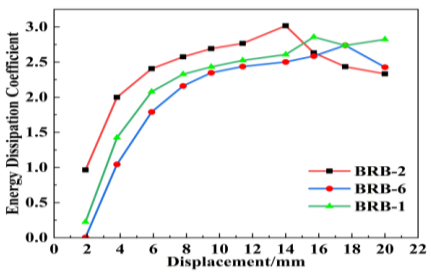

(a) Core Member Slenderness Ratio

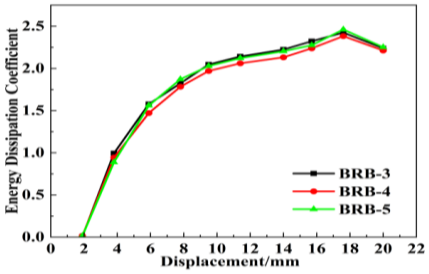

(b) Area ratio of the core tube to the tie rod

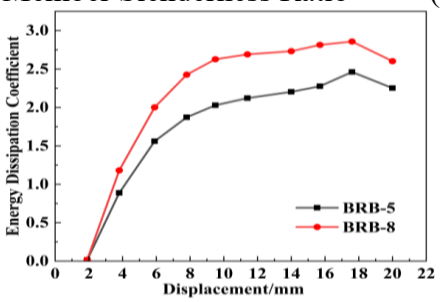

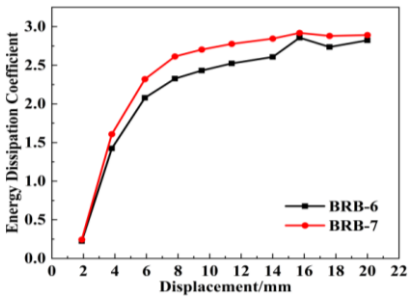

(c) Presence of tie rods

Figure 6. Energy dissipation coefficients of the hysteresis loops

3.3. Skeleton Curve Characteristics

The skeleton curves presented in Figure 7 demonstrate that all specimens exhibit typical three-stage mechanical behavior: Elastic stage: Constant initial stiffness, Elastoplastic stage: Gradual stiffness degradation, Plastic strengthening stage: Slow increase in load-bearing capacity. At 15mm displacement, all specimens reached peak load capacity, followed by stable strength degradation without sudden capacity drops, confirming the restraining system effectively prevents global instability. Key observations: Figure 7a: Initial elastic responses are nearly identical. Increased slenderness ratios delay peak displacement occurrence but reduce ultimate capacity by 8-12% due to necking effects. Higher slenderness improves member flexibility but increases local buckling risks. Figure 7b: <5% envelope curve variations indicate minimal cross-section area ratio influence on capacity. Area ratios primarily affect elastic stage stiffness redistribution with negligible plastic range impacts. Figure 7c: Tie rod-equipped specimens maintain consistent compressive capacity while demonstrating 32.1% higher tensile capacity versus non-tie rod specimens, proving the dual load-path mechanism's effectiveness in tension.

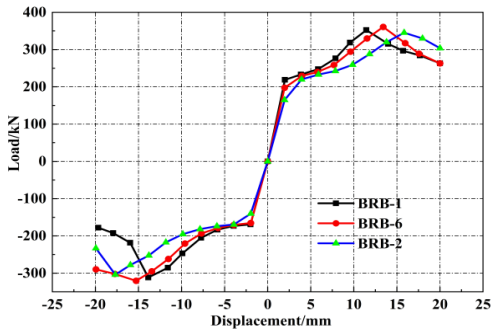

(a) Core Member Slenderness Ratio

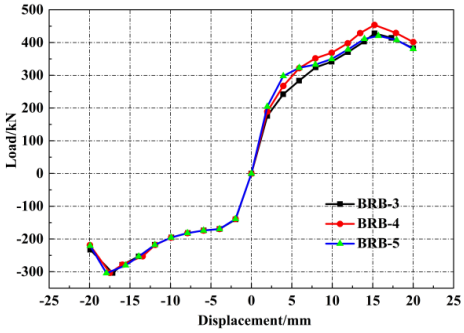

(b) Area ratio of the core tube to the tie rod

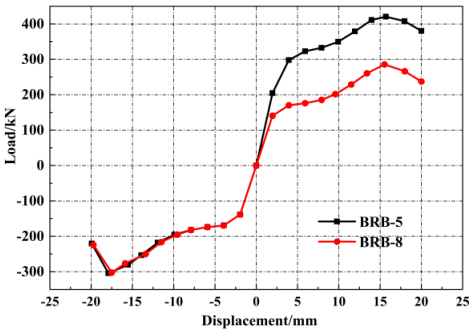

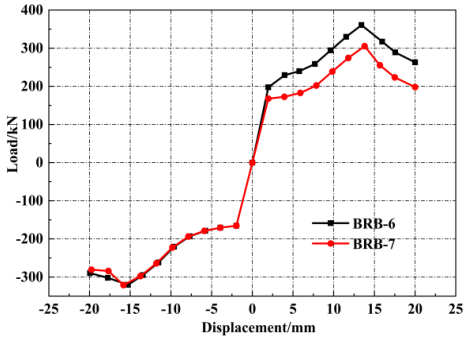

(c) Presence of tie rods

Figure 7. Skeletal curves of each component

The experimental data comparison between BRB-6/BRB-7 and BRB-5/BRB-8 models demonstrates significant performance improvements through tie rod implementation, with respective increases of 15.0% and 31.1% in initial stiffness, 21.9% and 43.9% in yield load, and 15.3% and 32.1% in peak load, conclusively proving the effectiveness of tie rods in enhancing both tensile stiffness and load-bearing capacity. Analysis of BRB-1, BRB-2 and BRB-6 models reveals an inverse relationship between slenderness ratio and initial stiffness, while yield and peak loads remain stable within ±5% variation range, accompanied by notable increases in yield and peak displacements, indicating that although higher slenderness reduces initial stiffness, it effectively delays structural yielding. The examination of BRB-3, BRB-4 and BRB-5 models shows a positive correlation between area ratio and initial stiffness, with less than 5% coefficient of variation in yield and peak loads and stable displacement parameters, confirming that area ratio primarily influences initial stiffness while having limited effect on ultimate load-bearing capacity.

Table 3. Mechanical Performance Indicators

Model No	Initial StiffnessK_0(kN/mm)	Yield Load F_y(kN)	Yield Displacement Δ_y(mm)	Peak LoadF_u(kN)	Peak DisplacementΔ_u(mm)
BRB-1	109.6	241.1	4.96	352.3	11.4
BRB-2	83.8	235.6	6.40	345.2	15.8
BRB-3	89.5	322.8	7.87	428.0	15.2
BRB-4	96.4	344.2	7.40	453.9	15.2
BRB-5	104.1	319.9	5.68	420.5	15.7
BRB-6	100.5	240.0	5.80	360.7	13.4
BRB-7	85.4	187.4	6.36	305.5	13.8
BRB-8	71.7	179.6	6.69	285.7	15.5

3.4. Stiffness Degradation Characteristics

The stiffness degradation curves in Figure 8 reveal that all models exhibit smooth and continuous stiffness reduction under cyclic loading without abrupt changes, indicating fully developed plastic deformation in the braces. Comparative analysis of BRB-1, BRB-2, and BRB-6 demonstrates an inverse relationship between core tube slenderness ratio and initial stiffness, where higher slenderness ratios result in lower initial stiffness values. During early loading stages, specimens with smaller slenderness ratios show faster stiffness degradation rates, while the degradation stabilizes in later stages. Increased slenderness ratios reduce initial stiffness by decreasing section moment of inertia but improve plastic deformation compatibility. Examination of BRB-3, BRB-4, and BRB-5 models shows nearly identical stiffness degradation patterns, confirming that cross-sectional area ratio variations primarily affect initial stiffness distribution with minimal influence on the degradation process. Comparisons between BRB-5/BRB-8 and BRB-6/BRB-7 indicate that tie rod implementation enhances initial stiffness while maintaining consistent stiffness degradation trends throughout loading.

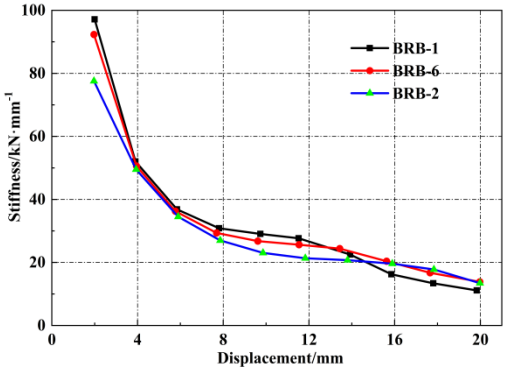

(a) Core Member Slenderness Ratio

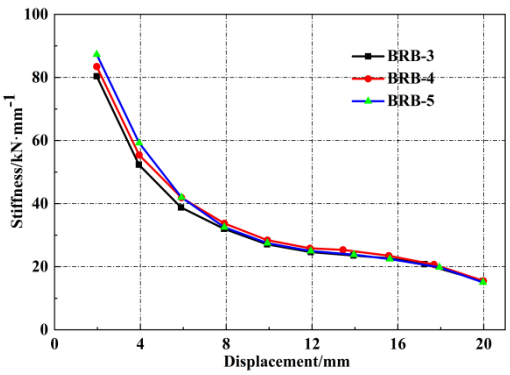

(b) Area ratio of the core tube to the tie rod

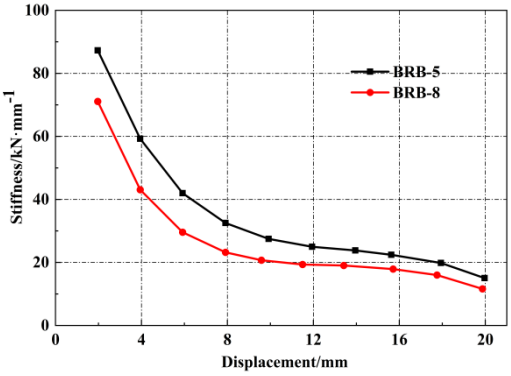

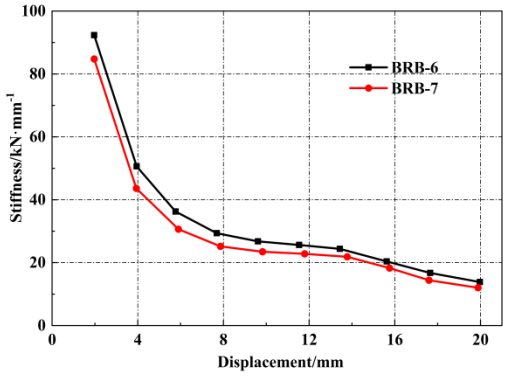

(c) Presence of tie rods

Figure 8. Secant Stiffness Degradation curves of the specimens

As shown in Figure 9, all models demonstrate significant plastic deformation capacity, with an average stiffness degradation magnitude reaching approximately 82.5%. The stiffness degradation of all specimens exceeds 80%, confirming that the bracing system exhibits excellent plastic deformation capability and can fully develop hysteretic energy dissipation.

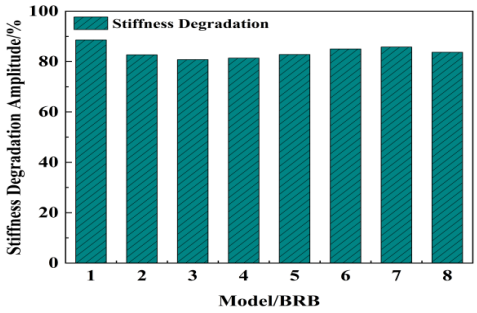

Figure 9. Amplitude of Secant Stiffness Degradation

3.5. Stress Evolution and Deformation Mechanism Analysis

Figure 10 systematically illustrates the complete mechanical response of the restrained buckling brace under cyclic loading. In compression, the load is solely resisted by the core tube with uniform stress distribution, while in tension, a dual-path load-transfer mechanism is activated through combined action of the core tube and high-strength tie rods. The core tube yields first, followed by yielding of the tie rods, exhibiting three distinct stress development phases: elastic stage, yielding stage, and plastic strengthening stage. Initial first-order buckling modes emerge at Δ=10mm loading displacement (Figure 10b) with maximum deflection reaching 12mm. Subsequent cyclic loading induces necking at the maximum moment section, ultimately developing alternating wrinkles in the necking zone (Figure 10f) that precipitate rapid load-bearing capacity degradation.

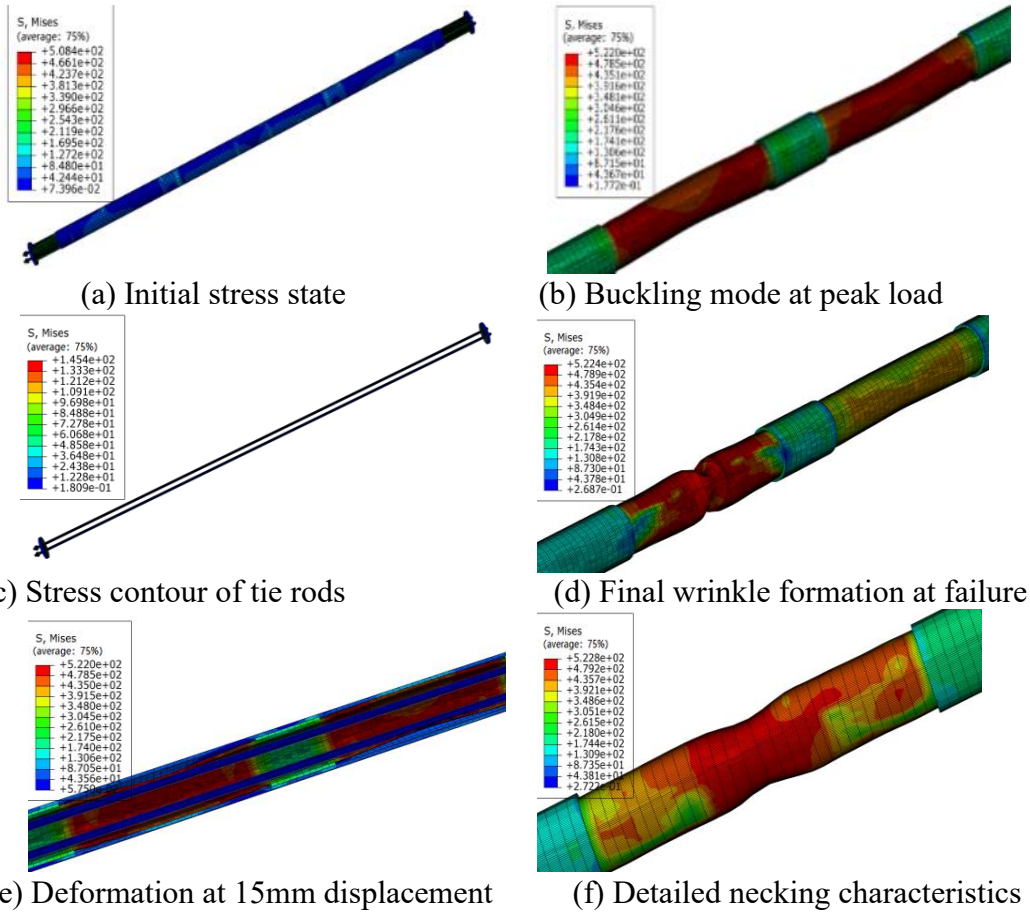

(a) Initial stress state (b) Buckling mode at peak load

(c) Stress contour of tie rods (d) Final wrinkle formation at failure

(e) Deformation at 15mm displacement (f) Detailed necking characteristics

Figure 10. Stress Distribution and Deformation Patterns of the Brace

4. Conclusion

This study systematically investigated the hysteretic energy dissipation characteristics and mechanical response of restrained buckling braces with movable high-strength tie rods under cyclic loading through ABAQUS nonlinear finite element analysis. The main conclusions are as follows:

(1) The incorporation of high-strength tie rods significantly enhances the tensile stiffness and load-bearing capacity of the brace. Compared to braces without tie rods, the initial tensile stiffness increases by 15.0%–31.1%, the yield load improves by 21.9%–43.9%, and the peak load rises by 15.3%–32.1%. The tie rods create a dual-path load-transfer mechanism under tension, suppressing necking development and resulting in peak-enhanced hysteresis loops, while also delaying stiffness degradation in compression.

(2) Increasing the slenderness ratio reduces initial stiffness but improves energy dissipation coefficients by 12%–18% through enhanced plastic deformation compatibility. Controlling the slenderness ratio within 1.2–2.4 balances stiffness and ductility requirements. Reducing the core tube-to-tie rod area ratio increases tensile capacity by 9.7%–15.2% but has minimal impact on compressive performance. Optimization of the area ratio should prioritize both tensile strengthening effects and material efficiency.

(3) Braces equipped with tie rods exhibit stable and well-developed hysteresis loops, with energy dissipation coefficients exceeding 2.0, meeting the "excellent" energy dissipation grade specified in seismic codes. The failure mode involves coordinated yielding of the core tube and tie rods in tension, and progressive buckling with localized necking in compression. The final failure pattern shows alternating wrinkles without global instability, confirming the effectiveness of the restraining system.

(4) The brace demonstrates significant tension-compression asymmetry, with tensile strength and stiffness 32.1% and 31.1% higher than compressive values, respectively. This asymmetric behavior provides new insights for optimizing composite bracing systems. For seismic design, it is recommended to utilize the tensile strengthening effect as the primary energy dissipation mechanism while improving compressive stability through tie rod pre-tensioning.

References

[1] Duan Liusheng, Su Mingzhou, Hao Kunlin, et al. Experimental study on the seismic performance of high-strength steel composite K-shaped eccentric braces in steel frames. Journal of Building Structures, 2014, 35 (07): 18-25.

[2] Yin Zhanzhong, Chen Wei, Chen Shenglin, et al. Experimental study on improved double steel tube buckling-restrained braces. Journal of Building Structures, 2014, 35 (09): 90-97.

[3] Mengsi W, Kejian M, Bo Y, et al. Experimental and numerical studies of multi-tube assembled buckling-restrained braces. Thin-Walled Structures, 2024, 195: 11453-.

[4] Yongsheng C, Yun Z, Shiyu T, et al. Performance of novel perforated double-core steel-plate assembled buckling-restrained braces. Journal of Building Engineering, 2024, 82: 108326-.

[5] He Jinzhou, Jia Mingming, Lv Dagang, et al. Energy dissipation and seismic performance of rocking truss-BRB-steel frame system. Journal of Building Structures, 2017, 38 (S1): 34-40.

[6] Zhou Ying, Shen Jiaohao, Xiao Yi. Review and prospects of self-centering energy dissipation braces. Journal of Building Structures, 2021, 42 (10): 1-13.

[7] Jia Mingming, Lv Dagang, Yu Xiaohui. Experimental study on the hysteretic performance of I-section non-yielding segment buckling-restrained braces. Journal of Civil Engineering, 2014, 47 (S2): 69-73.

[8] Guo Yanlin, Zhang Bohao, Wang Xiaoan, et al. Research progress on the design theory of prefabricated buckling-restrained braces. Journal of Building Science and Engineering, 2013, 30 (01): 1-12.

[9] Cheng Guangyu, Ye Lieping, Cui Hongchao. Design method of buckling-restrained energy dissipation steel braces. Journal of Building Structures, 2009, (1): 40-48.

[10] Guowei Z, Yongkun C, Jincheng S, et al. Seismic fragility analysis of rocking buckling-resistant braced structures subjected to far-field and near-field ground motions. Structures, 2023, 58.

[11] Guo Yanlin, Wang Xiaoan, Jiang Zhiqin, et al. Seismic performance of buckling-restrained brace with air-cooled island structure system. Journal of Building Science and Engineering, 2011, 28 (04): 9-18.

[12] Chaozhong Z, Shaojun Z, Shaohan Z, et al. Experimental and numerical investigations on an assembled self-centering buckling-restrained brace with high post-yield stiffness. Thin-Walled Structures, 2023, 190.

[13] Guo Yanlin, Liu Jianbin, Cai Yanyu, et al. Energy dissipation and seismic performance of buckling-restrained braces in structures. Building Structure, 2005, (08): 18-23.

[14] Gu Luzhong, Gao Xiangyu, Xu Jianwei, et al. Experimental study on the seismic performance of buckling-restrained braces in concrete frame structures. Journal of Building Structures, 2011, 32 (07): 101-111.

[15] Wu Hui, Zhang Guowei, Zhao Jian, et al. Experimental study on the seismic performance of buckling-restrained braces in existing RC frame structures. Journal of Civil Engineering, 2013, 46 (07): 37-46.

[16] Yin Zhanzhong, Wang Xiuli. Experimental study on a new type of double steel tube buckling-restrained brace. Building Science, 2011, 27 (03): 55-58.

[17] Song Yu. Civil Engineering Testing. Beijing: China Architecture & Building Press, 2011.

[18] Fan Jiajun, Wu Gang, Feng Decheng, et al. Experimental study and finite element analysis of the hysteretic performance of a new type of energy dissipation damper. Journal of Southeast University (Natural Science Edition), 2019, 49 (03): 413-419.

[19] Specification for Seismic Testing of Buildings: JGJ 101-1996 [S], 1996.